Inorganica Chimica Acta 589 (2026) 122948

Contents lists available at ScienceDirect

Inorganica Chimica Acta

journal homepage: www.elsevier.com/locate/ica

Synthesis, characterizacion and study of novel heterobimetallic RAPTA-type Ru(II) complexes

Nazanin Kordestani [a], Alvaro Martinez-Aguilera [a], Elisa Abas [b], Laura Grasa [b,c,d], Franco Scalambra [a,*], Antonio Romerosa [a,*]

[a] Department of Chemistry and Physics, Universidad de Almería, La Cañada, 04120, Almería, Spain
[b] Department of Pharmacology, Physiology, and Legal and Forensic Medicine, Universidad de Zaragoza, Miguel Servet, 50013, Zaragoza, Spain
[c] Aragón Health Research Institute (IIS Aragón), San Juan Bosco, 50009, Zaragoza, Spain
[d] Aragón Agri-Food Institute -IA2- (Universidad de Zaragoza–CITA), Miguel Servet, 50013, Zaragoza, Spain

ARTICLE INFO

Dataset link: SI Nasi-Alvaro-3.9 (Original data)

Dedicated to Prof. Francesco Vizza

Keywords:
RAPTA-like complexes
heterobimetallic complexes
Ruthenium
Copper
Palladium
PTA
dmoPTA
Antiproliferative activity

ABSTRACT

The new monometallic RAPTA complex $[RuCl_2(\eta^6\text{-}p\text{-cym})(dmPTA\text{-}\kappa P)](CF_3SO_3)_2$ (**1**) and novel *heterobimetallic* complexes $[RuCl_2(\eta^6\text{-}p\text{-cym})\text{-}\mu\text{-}(dmoPTA)\text{-}(1\kappa P{:}2\kappa^2 N,N'\text{-}M(L)Cl_2)]$ (M = Cu (**3**); M = Cu, L = DMF (**3·3$_{DMF}$**); M = Pd (**4**)) have been synthesized and characterized (dmPTA = *N,N′*-dimethyl-1,3,5-triaza-7-phosphaadamantane; dmoPTA = 3,7-dimethyl-1,3,7-triaza-5-phosphabicyclo[3.3.1]nonane). The synthesized complexes have been fully characterized by elemental analysis and spectroscopic techniques. The crystal structure of the complexes **2**, **3·3$_{DMF}$** and **4** were determined by single-crystal X-ray diffraction. The stability of complexes was studied in water and DMSO at room temperature and 37 °C. The anticancer activity against intestinal Caco-2/TC7 cells was studied.

1. Introduction

Organometallic complexes based on ruthenium have received increased attention as potential anticancer drugs and catalysts [1–4]. Numerous organometallic ruthenium complexes have been reported and reviewed in several comprehensive reviews, which provide further insights into their structural and functional properties [5,6]. Among these, ruthenium-arene-PTA, also known as RAPTA (PTA = 1,3,5-triaza-7-phosphaadamantane) complexes are particularly well-known for their versatility and biological relevance [7].

The ligand PTA is a widely used water-soluble phosphine, first reported in 1974 by Daigle [8], which is characterized by its amphiphilic character. The attractiveness of such ligand with one soft phosphorus and three hard nitrogen atoms, arises from its strong binding capability and variable denticity, which enables it to serve as a versatile building block for the synthesis of coordination polymers [9–11]. Functionalization of PTA by *N,N′*-dimethylation affords the dicationic ligand *N,N′*-dimethyl-1,3,5-triaza-7-phosphaadamantane (dmPTA) [12], which reacts with protic solvents under mild conditions to give rise to the ligand 3,7-dimethyl-1,3,7-triaza-5-phosphabicyclo[3.3.1]nonane (dmoPTA). This ligand can coordinate by the soft P and the two hard NCH_3 atoms, allowing the synthesis of monometallic and, more interesting, of a variety of different Ru-dmoPTA-M *heterobimetallic* complexes. Recently we have reported a variety of *heterobimetallic* complexes containing this ligand, such as $[RuCp(PPh_3)_2\text{-}\mu\text{-dmoPTA-}1\kappa P{:}2\kappa^2 N,N'\text{-}MCl_2](CF_3SO_3)$ (M = Zn, Co), showing that the presence of a second metal improves significantly the antiproliferative activity (up to 200 times that of cisplatin for T-47D and WiDr human solid tumor cell lines) with respect to the starting monometallic Ru-dmoPTA complex [13–15].

In 2017 Dyson and co-workers synthesized a new series of bimetallic RAPTA complexes through amide-forming reactions between mononuclear ruthenium arene carboxylic acid and diamine compounds with diverse substituents linking the amine groups. These bimetallic complexes displayed a different mechanism of action than the monometallic

* Corresponding authors.
E-mail address: romerosa@ual.es (A. Romerosa).

https://doi.org/10.1016/j.ica.2025.122948
Received 1 August 2025; Received in revised form 6 October 2025; Accepted 8 October 2025
Available online 10 October 2025

starting complexes against cancer cells [16]. Nevertheless, bimetallic RAPTA complexes in which two monometallic units are linked through an arene group present certain limitations, such as restricted ability to incorporate different metals within the same molecule, as well as issues related to the size and solubility of the resulting complexes. Very recently we presented a new series of *heterobimetallic* RAPTA complexes of general formula $[RuCl_2(\eta^6\text{-}p\text{-cym})\text{-}\mu\text{-dmoPTA-}1\kappa P{:}2\kappa^2N,N'\text{-}MCl_2]$ (M = Zn, Co, Ni), in which the ligand dmoPTA is coordinated to Ru through its P atom while the NCH_3 atoms chelate the heterometallic centre M [17]. Also in this case, the incorporation of a second metal significantly enhanced the antiproliferative activity against human adenocarcinoma colon cancer cell line Caco-2/TC7 in comparison with the monometallic starting complex $[RuCl_2(\eta^6\text{-}p\text{-cym})\text{-}(\kappa P\text{-HdmoPTA})](CF_3SO_3)$, and also with cisplatin and RAPTA-C. These complexes exhibit different mechanism of action against the evaluated colon cancer cell line, and none of them displayed toxicity towards intestinal normal cells. Therefore, varying the nature of the second metal may increase the cytotoxicity of monometallic RAPTA complexes, maintaining limited effects on intestinal normal cells.

The aim of this work was to synthesize new heterometallic complexes based on the $[RuCl_2(\eta^6\text{-}p\text{-cym})(\text{dmoPTA-}\kappa P)]$ scaffold to gain deeper insight into the structural requirements necessary for this class of compounds to act as effective antiproliferative agents. With this objective, complexes incorporating Pd and Cu as the second metal were synthesized, and their stability was evaluated along with their antiproliferative activity against the colon cancer cell line Caco-2/TC7. The choice of metal combinations was dictated by the fact of the high biological activity and low toxicity of previously published heterometallic complexes containing Ru [18–29], Cu [30–32] and Pd [33–36] metals.

2. Experimental

2.1. Materials

All chemicals were reagent grade and, unless otherwise specified, were used as received from commercial suppliers. The solvents were all degassed and distilled according to standard procedures. All reactions and manipulations were routinely performed under a dry nitrogen atmosphere using standard Schlenk-tube techniques. The hydrosoluble phosphine PTA [8] and $dmPTA(CF_3SO_3)_2$ [12] and the complex $[Ru(\eta^6\text{-}p\text{-cym})Cl_2]_2$ [37] and $[RuCl_2(\eta^6\text{-}p\text{-cym})(\text{HdmoPTA-}\kappa P)](CF_3SO_3)$ [17] were prepared as described in the literature.

2.2. Physical measurements

All complexes were characterized by FT-IR, ^1H, $^{13}C\{^1H\}$, $^{31}P\{^1H\}$, ^{19}F NMR, elemental analysis (C, H, N, S) and single crystal X-ray diffraction analysis. Complexes **3**/**3**·**3**$_{\mathbf{DMF}}$ were also studied by thermogravimetric analysis. FT-IR spectra have been carried out on a Bruker ECO-ATR ALPHA spectrometer and the intensity of the bands has been indicated as: strong (s), medium (m), weak (w). ^1H, $^{13}C\{^1H\}$, $^{31}P\{^1H\}$ and ^{19}F NMR spectra were recorded on a Bruker DRX500 spectrometer operating at 500.13 MHz, 125.76 MHz, 202.46 MHz and 470.59 MHz respectively. Peak positions are relative to tetramethylsilane and were calibrated against the residual solvent resonance (^1H) or the deuterated solvent multiplet (^{13}C). Chemical shifts for $^{31}P\{^1H\}$ NMR were measured relative to external 85 % H_3PO_4 with downfield values taken as positive. Elemental analysis (C, H, N, S) were performed on a Fisons Instruments EA 1108 elemental analyser. TGA measurements were run on a TGA Q50, TA Instruments, under nitrogen with a temperature ramp of 1 °C/min from 25 to 600 °C under nitrogen atmosphere.

2.3. Synthesis of $[RuCl_2(\eta^6\text{-}p\text{-cym})(\text{dmPTA-}\kappa P)](CF_3SO_3)_2$ (1)

Into a solution of $[Ru(\eta^6\text{-}p\text{-cym})Cl_2]_2$ (100 mg, 0.163 mmol), in 4 mL of dichloromethane, silver trifluoromethanesulfonate (167.8 mg, 0.653 mmol) was added under inert atmosphere. A white precipitate quickly formed, and the resulting mixture was stirred during 3 h at room temperature covered from light. The white precipitate was filtered under an inert atmosphere through a pad of Celite and a solution of dmPTA $(CF_3SO_3)_2$ (158.5 mg, 0.327 mmol) in 6 mL of dry acetone was slowly added into the red solution. The resulting mixture was stirred for about 1 h at room temperature, during which it turned orange. To this solution, tetrabutylammonium chloride (181.5 mg, 0.653 mmol) was added, resulting in an orange-red coloration. After 1 h, the solution was filtered and totally evaporated under reduced pressure. The addition of 5 mL of ethanol to the oily solid formed led to the formation of a pale-orange precipitate, which was collected by filtration, washed with ethanol (3 × 5 mL), Et_2O (3 × 5 mL) and dried under vacuum.

Yield: 188.7 mg, 73.0 %. $S_{25°C,H2O}$ = decomposition in 30 min, $S_{25°C,DMSO}$ = 110.4 mg/cm^3. Anal. for $C_{20}H_{32}Cl_2F_6PN_3O_6RuS_2$ (791.56 g/mol): Calcd. C, 30.35 %; H, 4.07 %; N, 5.31 %; S, 8.10 %. Found: C, 29.88 %; H, 4.09 %; N, 5.22 %; S, 7.46 %. IR (ATR, cm^{-1}): 3025 (w), 2985 (w), 2934 (w), 1467 (w), 1249 (s), 1163 (m), 1102 (m), 1053 (w), 1029 (s), 952 (w), 913 (w), 873 (w), 775 (m), 760 (m), 638 (s). ^1H NMR (500.13 MHz, Acetone-d_6, 25 °C) δ (ppm): 1.23 (d, $^3J_{HH}$ = 6.9 Hz, 6H, $(CH_3)_2CHPh_{p\text{-cym}}$), 2.11 (s, 3H, $CH_3Ph_{p\text{-cym}}$), 2.76 (sp, $^3J_{HH}$ = 6.9 Hz, 1H, $CHPh_{p\text{-cym}}$), 3.64 (s, 6H, CH_3N_{dmPTA}), 4.52 (s, 2H, NCH_2P_{dmPTA}), 4.92 + 5.23 (d + d, $^2J_{HH}$ = 14.7 Hz, 2H + 2H, $CH_3NCH_2P_{dmPTA}$), 5.50 + 5.77 (d + d, $^2J_{HH}$ = 12.3 Hz, 2H + 2H, NCH_2N_{dmPTA}), 5.90 (s, 2H, $CH_3NCH_2N_{dmPTA}$), 6.03 (d, $^3J_{HH}$ = 6.0 Hz, 2H, ***ortho*-H**$_{p\text{-cym}}$), 6.08 (d, $^3J_{HH}$ = 6.0 Hz, 2H, ***meta*-H**$_{p\text{-cym}}$). $^{13}C\{^1H\}$ NMR (125.76 MHz, Acetone-d_6, 25 °C) δ (ppm): 17.54 (s, 1C, $CH_3Ph_{p\text{-cym}}$), 21.31 (s, 2C, $(CH_3)_2CHPh_{p\text{-cym}}$), 30.70 (s, 1C, $CHPh_{p\text{-cym}}$), 45.17 (d, $^1J_{PC}$ = 21.6 Hz, 1C, NCH_2P_{dmPTA}), 51.78 (s, 2C, CH_3N_{dmPTA}), 55.31 (d, $^1J_{PC}$ = 14.1 Hz, 2C, $CH_3NCH_2P_{dmPTA}$), 78.51 (s, 1C, $CH_3NCH_2N_{dmPTA}$), 78.81 + 78.84 (s + s, 1C + 1C, NCH_2N_{dmPTA}), 87.02 (d, $^2J_{PC}$ = 5.8 Hz, 2C, ***ortho*-C**$H_{p\text{-cym}}$), 90.25 (d, $^2J_{PC}$ = 5.6 Hz, 2C, ***meta*-C**$H_{p\text{-cym}}$), 99.48 (s, 1C, $CH_3C_{p\text{-cym}}$), 108.74 (s, 1C, $(CH_3)_2CHC_{p\text{-cym}}$), 120.89 (c, $^1J_{FC}$ = 320.1 Hz, 2C, $CF_3SO_3^-$). $^{31}P\{^1H\}$ NMR (202.46 MHz, Acetone-d_6 25 °C) δ (ppm): −15.99 (s, 1P, dmPTA). ^{19}F NMR (470.59 MHz, Acetone-d_6, 25 °C,) δ (ppm): −79,08 (s, $CF_3SO_3^-$).

2.4. Reviewed synthesis of $[RuCl_2(\eta^6\text{-}p\text{-cym})(\text{dmoPTA-}\kappa P)]\cdot(C_6H_5CH_3)_{0.5}$ (**2**$_{\mathbf{Tol}}$)

To a solution of $[RuCl_2(\eta^6\text{-}p\text{-cym})(\text{HdmoPTA-}\kappa P)](CF_3SO_3)$ (50 mg, 0.079 mmol) in 2 mL of dry methanol cooled to −20 °C, *t*-BuOK (8.9 mg, 0.079 mmol) was added. The resulting solution was stirred for about 15 min and then totally evaporated under reduced pressure. The addition of 0.5 mL of dry chloroform and 1.5 mL of toluene led to the precipitation of a triflate salt. After cooling to −20 °C, the resulting mixture was filtered through a pad of Celite, and the solution was concentrated under reduced pressure to 0.5 mL, resulting in the formation of a bright orange microcrystalline precipitate which was collected by filtration, washed with cold (< 5 °C) toluene (3 × 1 mL), Et_2O (3 × 3 mL) and dried under vacuum. Single crystals were obtained by slow evaporation from a $CHCl_3$/toluene (1:3) solution at 5 °C.

Yield: 16.4 mg, 43.2 %.

2.5. Synthesis of $[RuCl_2(\eta^6\text{-}p\text{-cym})\text{-}\mu\text{-dmoPTA-}1\kappa P{:}2\kappa^2N,N'\text{-}CuCl_2]$ (3) and $[RuCl_2(\eta^6\text{-}p\text{-cym}))\text{-}\mu\text{-dmoPTA-}1\kappa P{:}2\kappa^2N,N'\text{-}CuCl_2](DMF)\cdot[RuCl_2(\eta^6\text{-}p\text{-cym})\text{-}\mu\text{-dmoPTA-}\kappa P{:}2\kappa^2N,N'\text{-}CuCl_2(DMF\text{-}\kappa O)]$ (**3**·**3**$_{\mathbf{DMF}}$)

Into a solution of $[RuCl_2(\eta^6\text{-}p\text{-cym})(\text{dmoPTA})]$ (100 mg, 0.2 mmol) in 5 mL of dried MeOH, $CuCl_2\cdot 2H_2O$ (35.5 mg, 0.2 mmol) was added under inert atmosphere. A brown precipitate formed slowly, and the resulting mixture was stirred for 5 h at room temperature. The precipitate was filtered, washed with cold (< 5 °C) MeOH (3 × 1 mL) and Et_2O (3 × 1 mL) and dried under vacuum. Single crystals of **3**·**3**$_{\mathbf{DMF}}$ were obtained by vapor diffusion of Et_2O into a DMF solution of the compound.

Yield: 0.09 g, 70 %. $S_{25°C,H2O}$ = 9.5 mg/cm^3, $S_{25°C,DMF}$ = 41.2 mg/cm^3, $S_{25°C,DMSO}$ = 49.5 mg/cm^3. Anal. for powder sample $C_{17}H_{30}Cl_4PN_3RuCu{\cdot}H_2O$ (**3**) (631.85 g/mol): Cald: C, 32.31 %; H, 5.10 %; N, 6.65 %. Found: C, 31.87 %; H, 5.23 %; N, 6.60 %. Anal. for crystal sample $C_{37}H_{67}Cl_8P_2N_7ORu_2Cu_2{\cdot}DMF$ (**3·3$_{DMF}$**) (1373.87 g/mol): Cald: C, 34.97; H, 5.43; N, 8.16 %. Found: C, 34.85 %; H, 5.79 %; N, 8.46 %. IR of **3** (ATR, intense bands, cm^{-1}): 2968 (w), 2903 (w), 1629 (w), 1455 (m), 1380 (w), 1357 (w), 1256 (w), 1209 (w), 1134 (w), 1110 (w), 1065 (s), 1028 (w), 975 (m), 919 (w), 875 (w), 834 (s), 794 (w), 759 (w) 717 (w), 614 (m). IR of **3·3$_{DMF}$** (ATR, intense bands, cm^{-1}): 2969 (w), 2911 (w), 1675 (s), 1656 (s), 1571 (w), 1501 (w), 1455 (m), 1418 (w), 1383 (m), 1359 (w), 1257 (w), 1209 (w), 1134 (w), 1110 (w), 1090 (w), 1064 (s), 1029 (w), 976 (m), 874 (w), 836 (w), 798 (s), 717 (w), 699 (w), 666 (w), 614 (m). ^{1}H NMR of **3** (500.13 MHz, 25 °C, DMSO-d_6): 1.27–2.28 (m, 10H, **H *p*-cym**), 5.86–6.39 (m, 4H, **H aromatics**). ^{1}H NMR of **3·3$_{DMF}$** (500.13 MHz, 25 °C, DMSO-d_6): 1.02–2.39 (m, 10H, **H *p*-cym**), 2.73 (s, 3H, (C**H**$_3$)$_2$N$_{DMF}$), 2.89 (s, 3H, (C**H**$_3$)$_2$N$_{DMF}$), 5.63–6.80 (m, 4H, **H aromatics**), 7.96 (s, 1H, NC**H**O$_{DMF}$).^{13}C{^{1}H} NMR (125.76 MHz, 25 °C, DMSO-d_6): no signals were observed. ^{31}P{^{1}H} NMR of **3** (202.46 MHz, 25 °C, DMSO-d_6): δ(ppm) -9.09 (s, dmoPTA-$CuCl_2$). ^{31}P{^{1}H} NMR of **3·3$_{DMF}$** (202.46 MHz, 25 °C, DMSO-d_6): δ(ppm) -9.86(s, dmoPTA-$CuCl_2$DMF).

2.6. Synthesis of [$RuCl_2(\eta^6$-*p*-cym)-*μ*-dmoPTA-1*κP*:2*κ*^{2}*N,N′*-$PdCl_2$] (**4**)

To a solution of [$RuCl_2(\eta^6$-*p*-cym)(dmoPTA)] (100 mg, 0.2 mmol) in 5 mL of dry chloroform, Pd(*COD*)Cl_2 (59.5 mg, 0.2 mmol) was added under inert atmosphere. A yellow precipitate quickly formed, and the resulting mixture was stirred for 2 h at room temperature. The precipitate was filtered, washed with cold (< 5 °C) chloroform (3 × 1 mL) and Et_2O (3 × 1 mL) and dried under vacuum. Single crystals were obtained by slow evaporation of a DMSO solution of the compound.

Yield: 0.11 g, 80 %. $S_{25°C,H2O}$ = 7.8 mg/cm^3, $S_{25°C,DMF}$ = 35.3 mg/cm^3, $S_{25°C,DMSO}$ = 40.5 mg/cm^3. Anal. for $C_{17}H_{30}Cl_4PN_3RuPd$ (656.71 g/mol): Cald: C, 31.09 %; H, 4.60 %; N, 6.40 %. Found: C, 31.23 %; H, 4.11 %; N, 6.46 %. IR (ATR, intense bands, cm^{-1}): 3054 (w), 2966 (w), 2920 (w), 2847 (w), 1458 (m), 1448 (m), 1434 (w), 1380 (m), 1359 (w), 1271 (w), 1210 (w), 1133 (m), 1057 (s), 1037 (m), 972 (m), 913 (w), 879 (w), 833 (s), 764 (w), 728 (m), 617 (s). ^{1}H NMR (500.13 MHz, 25 °C, DMF-d_7): δ(ppm) 1.21 (d, $^3J_{HH}$ = 6.9 Hz, 6H, *(CH$_3$)$_2$*CHPh$_{p\text{-cymene}}$), 2.08 (s, 3H, *CH$_3$*Ph$_{p\text{-cym}}$), 2.58 + 2.59 (s + s, 3H + 3H, *CH$_3$*N$_{dmoPTA}$), 2.72 (septet, $^3J_{HH}$ = 6.9 Hz, 1H, *CH*Ph$_{p\text{-cym}}$), 3.41 (bs, 2H, P*CH$_2$*N$_{dmoPTA}$), 3.48 + 4.44 (m + m, 2H + 2H, CH$_3$N*CH$_2$*P$_{dmoPTA}$), 3.89 + 4.65 (d + d, $^2J_{HH}$ = 12.6 Hz, 2H + 2H, N*CH$_2$*N$_{dmoPTA}$), 6.06 (m, $^3J_{HH}$ = 5.5 Hz, 4H, aromatics *p*-cym); ^{13}C{^{1}H} NMR (125.76 MHz, 25 °C, DMF-d_7): δ(ppm) 18.36 (s, *CH$_3$*Ph$_{p\text{-cym}}$), 21.53 (s, *(CH$_3$)$_2$*CHPh$_{p\text{-cym}}$), 31.47 (s, *CH*Ph$_{p\text{-cym}}$), 42.73 (d, $^1J_{PC}$ = 6.89 Hz, N*CH$_2$*P$_{dmoPTA}$), 54.20 (bs, *CH$_3$*N$_{dmoPTA}$), 55.11 (bd, CH$_3$N*CH$_2$*P$_{dmoPTA}$), 75.03 (s, NCH$_2$N$_{dmoPTA}$), 80.33 (s, ortho-*CH$_p$*$_{\text{-cym}}$), 89.73 (s, meta-*CH$_p$*$_{\text{-cym}}$), 120.35 (s, CH$_3$*C$_p$*$_{\text{-cym}}$), 122.91 (s, (CH$_3$)$_2$CH*C$_p$*$_{\text{-cym}}$); ^{31}P{^{1}H} NMR (202.46 MHz, 25 °C, DMF-d_7): δ(ppm) -11.15 (s, dmoPTA-$PdCl_2$).

2.7. Single crystal X-Ray diffraction

Single crystal X-ray diffraction was performed with a Bruker APEX-II CCD diffractometer at 100 K for **2$_{Tol}$**, **3·3$_{DMF}$** and **4** using MoK_α radiation. Data was integrated (SAINT, Bruker) an scaled (SADABS, Bruker) and finally the structure was solved with SHELXT [38] using intrinsic phasing and refined with SHELXL [39] by least squares. Solution and refinement procedures were accomplished by Olex2 software [40]. The crystal structures have been deposited at CSD with CCDC numbers 2475961 (**2$_{Tol}$**), 2475963 (**3·3$_{DMF}$**), 2475962 (**4**) Crystallographic and structural data are given in tables **S1-S7**.

2.8. Stability tests

All experiments were performed by a similar procedure: the complex (0.005 g) was introduced into a 5 mm NMR tube and dissolved in 0.4 mL of degassed solvent (D_2O or DMSO). Into the resulting solution, filtered air was gently bubbled throughout for 2 min. The solutions were left at room temperature and monitored by ^{31}P{^{1}H} NMR first every 30 min and later in longer time periods. A similar experiment was performed but the final temperature was set at 37 °C.

2.9. ESI-MS measurements

Stock solutions of 3.5 mg of complexes **1**, **3** and **4** in 0.4 mL of D_2O were prepared. The solutions were left at 37 °C for up to 72 h. From the dissolutions, 10 μL were taken and diluted to 10 mL with MS-grade MeOH prior to direct injection into an AB Sciex QTRAP 4500 mass spectrometer operating in positive or negative mode.

2.10. Biological studies

2.10.1. Cell culture

This study was carried out in the human enterocyte-like cell line Caco-2/TC7 [41]. This cell line undergoes in culture a process of spontaneous differentiation that leads to the formation of a monolayer of cells, expressing the morphological and functional characteristics of mature enterocytes. This differentiation process is growth-dependent, where the cells undergo differentiation from undifferentiated proliferative crypt-type cells' in exponential phase of growth, to differentiated enterocyte-type cells' in stationary phase [42]. The cell culture of Caco-2/TC7 cells (passages 30–50) were carried out according to a previously reported method [43,44]. Caco-2/TC7 cells were cultured at 37 °C in an atmosphere of 5 % CO_2 and maintained in high glucose DMEM supplemented with 2 mM glutamine, 100 U/mL penicillin, 100 μg/mL streptomycin, 1 % nonessential amino acids, and 20 % heat-inactivated fetal bovine serum (FBS) (Life Technologies, Carlsbad, CA, USA). Thus, experiments in undifferentiated and differentiated cells (considered as cancer and normal cells, respectively) were performed on day 5 and day 15 post-seeding, respectively. For cell viability assays, cells were seeded in 96-well plates at a density of 2 × 10^4 or 4 × 10^3 cells per well, and measurements were carried out 5 or 15 days after seeding, respectively. For apoptosis and cell cycle analyses at 3 × 10^4 cells/cm^2; and for caspase assays at 10^3 cells per well in 96-well plates. Stock solutions of the complexes (in DMSO) were diluted in the complete medium to the required concentration. DMSO at similar concentrations did not show any cytotoxic effects. The culture medium was replaced with fresh medium (without FBS) containing the complexes at concentrations varying from 0 to 20 μM, and with an exposure time of 72 h for cell viability assays. For all the other studies, the cells were incubated at 20 μM for 24 h.

2.10.2. Cell viability assay

Cell survival was measured using the MTT test [45]. The assay depends on the cellular reduction of 3-(4,5-dimethylthiazol-2-yl)-2,5-diphenyltetrazolium bromide (MTT, Sigma-Aldrich, Madrid, Spain) by the mitochondrial dehydrogenase of viable cells to a blue formazan product that can be measured spectrophotometrically, as it was previously described [10,11]. After 72 h of incubation with or without the metallic complexes, MTT (5 mg mL^{-1}) was added to each well in an amount equal to 10 % of the culture volume. Cells were incubated with MTT at 37 °C for 3 h. After that, the medium and MTT were removed and 100 μL of DMSO was added to each well. The plate was gentle stirred in a shaker. Finally, the cell viability was determined by measuring the absorbance with a multiwell spectrophotometer SPECTROstar Nano Absorbance Reader (BMG LabTech) at a wavelength of 560 nm and compared with the values of control cells incubated in the absence of the complexes. IC_{50} values were calculated using a conventional

concentration – response curve with variable slope. Experiments were conducted in quadruplicate wells and repeated at least three times.

3. Results and discussion

3.1. NMR characterization of complexes 1, 3/3·3$_{DMF}$ and 4

The monometallic complex [$RuCl_2$(η^6-*p*-cym)(dmPTA-κ*P*)](CF_3SO_3)$_2$ (**1**) was prepared by a three-step reaction via the initial [Ru(η^6-*p*-cym)Cl_2]$_2$ chloride abstraction by an molar excess of $AgCF_3SO_3$ in dichloromethane, followed by the addition of an equivalent of the ligand dmPTA (CF_3SO_3)$_2$ in dry acetone, and the reaction with [(*n*-Bu)$_4$N]Cl, which provided the chloride needed to complete the coordination geometry around the metal (Scheme 1). All efforts to obtain the complex without using $AgCF_3SO_3$ and [(*n*-Bu)$_4$N]Cl, required heating the reaction at reflux temperature, which gave rise to a mixture of compounds **1** and **a**.

The $^{31}P\{^1H\}$ NMR spectrum of **1** (**Fig. S4**) shows a unique singlet at −15.99 ppm in acetone-d_6, ca. 10 ppm shifted to upfield with respect to the deprotonated analogue opened-cage complex [$RuCl_2$(η^6-*p*-cym)(dmoPTA-κ*P*)] (−5.99 ppm) [17]. The ^1H NMR spectrum of **1** displays the protons of dmPTA at downfield and in a wider range (3.64–5.90 ppm, **Fig. S2**) than the range observed for the dmoPTA (2.30–3.84 ppm) [17] with two additional protons corresponding to the signal of CH_2 group between the quaternary nitrogen atoms (5.90 ppm, **Fig. S2**). The *p*-cymene signals do not suffer significant variations except for the inequivalent aromatic protons which give rise to two coupled doublets (6.03–6.08 ppm, **Fig. S2**). The $^{13}C\{^1H\}$ NMR spectrum of **1** (**Fig. S3**) displays also the expected signals for the CH_2 group between the quaternary nitrogen atoms (78.51 ppm, **Fig. S3**) assigned by means of ^1H—^{13}C HSQC NMR (**Fig. S7**). The presence of the $CF_3SO_3^-$ anion was supported by ^{19}F NMR (−79.08 ppm; **Fig. S5**) and FT-IR (ν_{SO} = 1249 cm^{-1}) (**Fig. S1**). Finally, the elemental analysis of complex **1** agrees with its proposed structure.

Despite the synthesis of the complex [$RuCl_2$(η^6-*p*-cym)(dmoPTA-κ*P*)] (**2**) has been published previously [17], a reviewed synthesis was carried out to obtain crystals for the determination of its structure by single crystal X-ray diffraction, that will be discussed later. Reaction of complex [$RuCl_2$(η^6-*p*-cym)(HdmPTA-κ*P*)](CF_3SO_3) (**a**) with t-BuOK in dry MeOH at −20 °C affords the deprotonation of the HdmoPTA ligand. Removal of the KCF_3SO_3 by dissolving the complex in a $CHCl_3$/toluene (1:3) mixture afforded complex [$RuCl_2$(η^6-*p*-cym) (dmoPTA-κ*P*)]·($C_6H_5CH_3$)$_{0.5}$ (**2$_{Tol}$**).

The *heterobimetallic* complexes [$RuCl_2$(η^6-*p*-cym)-μ-dmoPTA-1κ*P*:2κ^2*N,N′*-MCl_2] (M = Cu (**3**), Pd (**4**)) were synthesized by reaction (Scheme 1) of the starting complex [$RuCl_2$(η^6-*p*-cym)(dmoPTA-κ*P*)] (**2**) [17] with $CuCl_2$ and [Pd(*COD*)Cl_2] in dry MeOH and $CHCl_3$, respectively. The $^{31}P\{^1H\}$ NMR spectra of the *heterobimetallic* complexes **3** and **4** show a unique singlet at −9.09 (DMSO-d_6) and − 11.15 ppm (DMF-d_7) respectively (**Fig. S12**, **S18**), which arise at higher field than in the starting complex **2** (−5.99 ppm). [17] This behaviour was observed also in the similar *heterobimetallic* complexes [$RuCl_2$(η^6-*p*-cym)-μ-dmoPTA-1κ*P*:2κ^2*N,N′*-$ZnCl_2$] [17] and [$RuCp(PPh_3)_2$-μ-dmoPTA-1κ*P*:2κ^2*N,N′*-$ZnCl_2$](CF_3SO_3) [14].

Recrystallization of complex **3** from DMF resulted in the formation of crystals of **3·3$_{DMF}$**, which were constituted with two different Ru—Cu dimetallic complexes. Both of them are constituted by a {$RuCl_2$(η^6-*p*-cym)-μ-dmoPTA-1κ*P*:2κ^2*N,N′*} moiety that is linked by the CH_3N_{dmoTA} atoms to a Cu, which is a distorted tetrahedral Cu center coordinated to two chloride (complex **3**). One DMF molecule is located nearby but is not coordinated to the metal. The other complex (**3$_{DMF}$**) consists of a five-coordinated Cu(II) bonded to two chloride and one DMF molecule by its O atom, exhibiting a distorted trigonal-bypiramidal geometry (Fig. 1).

The ^1H NMR spectra of complexes **3** and **3·3$_{DMF}$** (**Fig. S10**, **S11**) are influenced by the paramagnetic nature of the Cu(II) centre, which particularly affects the CH_3N_{dmoPTA} protons, rendering them undetectable in the recorded spectra. This observation supports the coordination of these atoms to the metal centre. The influence of the metal is significantly reduced but still observable in the *p*-cymene protons, which appear as a broad signal in the range 5.63–6.80 in both complexes. The FT-IR spectrum (**Fig. S9**) is in agreement with the presence of a coordinated and a solvate DMF molecules, given that two bands at 1675 and 1656 cm^{-1} ($\nu_{c=o}$) are observed in agreement with the bibliography [46,47]. It is important to highlight that these bands are not observed in the IR spectrum of complex **3** (**Fig. S8**). Finally, the elemental and thermogravimetric analysis of complexes **3** and **3·3$_{DMF}$** agree with their structure (**Fig. S14**).

In contrast, the ^1H NMR spectra of the Ru—Pd complex **4** (**Fig. S16**) shows signals corresponding to the *p*-cymene and dmoPTA ligands at the expected chemical shift [6,48]. In comparison with starting complex **2**,

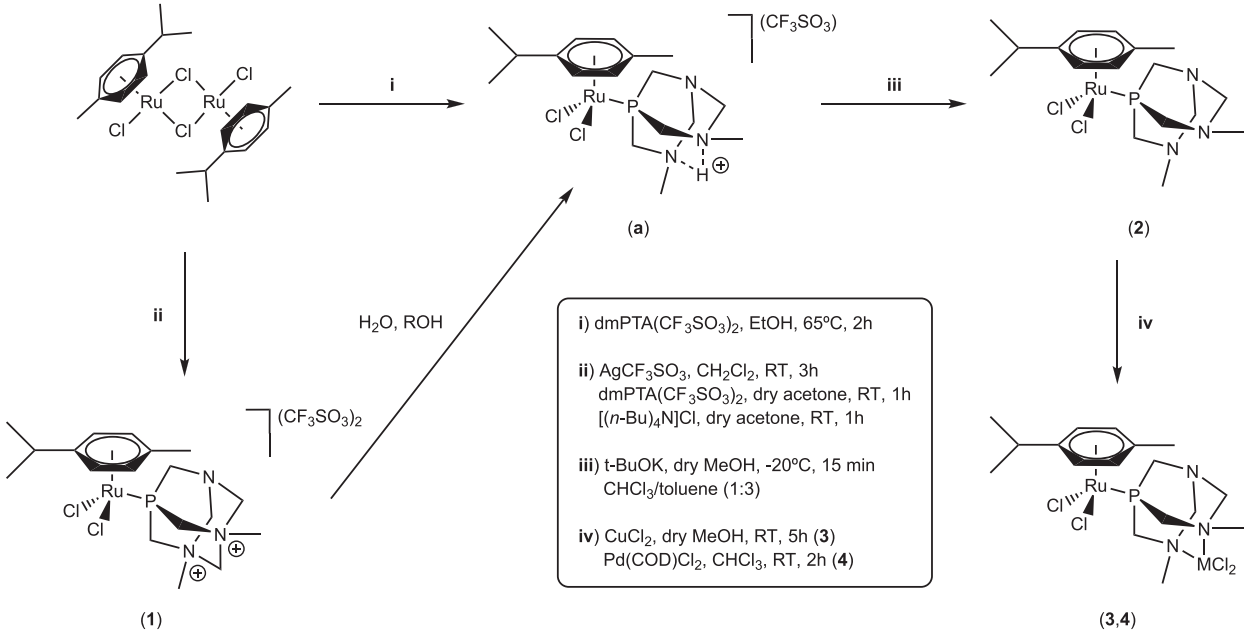

Scheme 1. Synthesis of **1–4**.

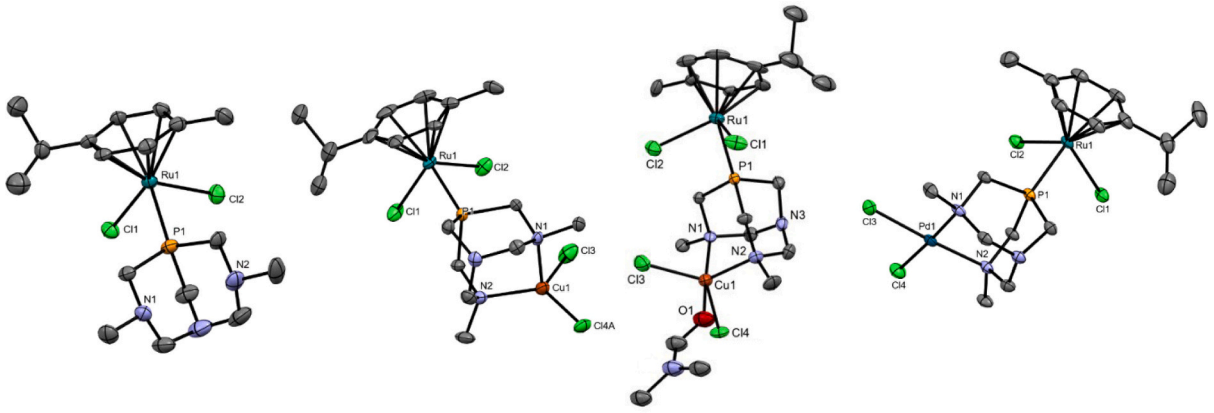

Fig. 1. Crystal structure of **2**, **3·3$_{DMF}$** and **4** (ellipsoids at 50 % probability. Hydrogen atoms, anions and solvent molecules were omitted for clarity).

the ^{1}H NMR spectrum of **4** shows the dmoPTA protons shifted to downfield (3.56–4.83 ppm) while not any significant change is observed for the *p*-cymene protons, supporting the coordination of CH_3N_{dmoPTA} atoms by a diamagnetic metal such as Pd(II). The $^{31}P\{^{1}H\}$ (**Fig. S18**) and $^{13}C\{^{1}H\}$ NMR (**Fig. S17**) of **4** displays the expected signals for the proposed structure as well as its elemental analysis and IR (**Fig. S15**).

3.2. *Crystal structures of complexes **2$_{Tol}$**, **3·3$_{DMF}$** and **4***

Although the synthesis of the complex [$RuCl_2$(η^6-*p*-cym)(dmoPTA-κ*P*)] has been previously reported [17], its characterization was proposed by spectroscopic methods, as suitable single crystals for X-ray diffraction could not be obtained at that time. The crystal structure of this complex is significant, as this compound serves as the starting point for synthesis of the subsequent heterometallic complexes. Thus, comparing their crystal structures the complex may provide key information into the factors underlying their structure-activity relationship. After multiple attempts, suitable single crystals were obtained by slow evaporation of a solution of the complex in $CHCl_3$/toluene (1:3) at 5 °C. Multiple attempts were also required to obtain single crystals of **3·3$_{DMF}$** and **4**. Brown single crystals of **3·3$_{DMF}$** were obtained by vapor diffusion of diethyl ether into a DMF solution of the complex, whereas single crystals of **4** were grown by slow evaporation of its solution in DMSO. Selected bond distances and angles for complex **2$_{Tol}$**, **3·3$_{DMF}$** and **4** are summarized in Table 1.

The crystal structure of complexes **2**–**4** (Fig. 1) fully supported their proposed composition. Bright-orange single crystals of complex [$RuCl_2$(η^6-*p*-cym)(dmoPTA-κ*P*)]·($C_6H_5CH_3$)$_{0.5}$ (**2$_{Tol}$**) crystalized in the space group $P2_12_12_1$. The asymmetric unit is constituted by one neutral ruthenium complex [$RuCl_2$(η^6-*p*-cym)(dmoPTA-κ*P*)] and half disordered molecule of toluene solvate. The distorted pseudo-octahedral coordination sphere around the Ru atom is constituted by one η^6-coordinated *p*-cymene, two chloride ions and one dmoPTA ligand coordinated by the phosphorus atom. The bond distances and angles in the dmoPTA ligand are in agreement with those found in analogue complexes [49]. The Ru1-*p*-cymene-centroid bond distance and *p*-cymene-Ru1-L (L = P, Cl) angles (Ru1-*p*-cym$_{cent}$: 1.694 Å; mean *p*-cym-Ru1-L angles: 85.19(5)°) are similar to those found in analogue complexes [17]. The absence of the hydrogen between the CH_3N_{dmoPTA} atoms leads to a dealignment of the methyl groups (C6-N1-N2-C7 dihedral angle: 6.68°) with respect to complex [$RuCl_2$(η^6-*p*-cym)(HdmoPTA-κ*P*)](CF_3SO_3) (C6-N1-N2-C7 dihedral angle: 2.48°), as well as an elongation of 0.241 Å of the distance between the CH_3N atoms (**2**: 2.954(1) Å, [$RuCl_2$(η^6-*p*-cym)(HdmoPTA-κ*P*)](CF_3SO_3): 2.713(1) Å) [17]. This behaviour already shows that the dmoPTA ligand is a better chelator for a second metal centre than the HdmoPTA ligand [48].

Table 1
Selected bond lengths and angles for complexes **2**, **3·3$_{DMF}$** and **4**.

	2	**3·3$_{DMF}$**	**4**
Length (Å)			
Ru1-Cl1	2.411(2)	2.407(2)/2.410(2)	2.414(8)
Ru1-Cl2	2.412(2)	2.406(2)/2.411(2)	2.412(9)
Ru1-P1	2.309(3)	2.291(2)/2.301(2)	2.300(8)
Ru1-*p*cym$_{cent}$	1.694	1.704/1.697	1.718
N1-N2	2.954	2.864/2.894	2.946
M^b-Cl3		2.215(5)/ 2.323(3)	2.305(9)
M^b-Cl4		2.257(3)/2.351(4)	2.294(9)
M^b-N1		1.994(7)/2.034(7)	2.095(3)
M^b-N2		2.024(7)/ 2.105(7)	2.101(3)
M^b-O1$_{DMF}$		2.241(8)/2.001(9)	
Angle (°)			
Cl1-Ru1-Cl2	90.21(9)	86.83(9)/ 86.23(9)	87.38(3)
P1-Ru1-Cl1	83.03(9)	87.92(8)/88.24(8)	85.03(3)
P1-Ru1-Cl2	82.34(9)	84.62(8)/85.61(8)	84.96(3)
P1-Ru1-*p*cym$_{cent}$	132.27	129.39/128.28	129.91
Cl3-M^b-Cl4		117.42(16)/123.58(14)	85.66(3)
N1-M^b-N2		90.9(3)/88.7(3)	89.18(10)
N1-M^b-Cl3		108.65(2)/95.2(2)	92.29(8)
N1-M^b-Cl4		116.9(2)//95.6(2)	177.46(8)
N2-M^b-Cl3		117.7(3)/121.6(2)	174.92(8)
N2-M^b-Cl4		102.5(2)/113.9(2)	92.73(8)
M^b-N1-C6		105.4(5)/108.7(5)	115.4(2)
M^b-N2-C7		110.3(5)//113.9(5)	115.7(2)
Dihedral angle	6.68	0.35/1.92	1.79

The *heterobimetallic* complexes **3·3$_{DMF}$** crystallized in the space group $P2_1$. As indicated previously, the compound **3·3$_{DMF}$** is constituted by two different Ru—Cu complex units. The first molecule (**3**) is constituted by the complex unit of **2**, the {$RuCl_2$(η^6-*p*-cym)(dmoPTA-κ*P*)} moiety, bonded by its CH_3N_{dmoPTA} atoms to a distorted tetrahedral Cu coordinate to two chloride ions. Nearby to the complex there is one DMF molecule at a distance (Cu1-O$_{DMF}$ = 2.241 Å) shorter than the sum of their Van der Waals radii [50]. The second molecule in the crystal is made by the same pseudo-octahedral Ru moiety bonded by the CH_3N_{dmoPTA} atoms to a distorted trigonal-bypiramidal Cu(II) that completes its coordination geometry by two chlorides, as complex **3**, but also to a DMF molecule by the O atom, which is *trans* to one of the CH_3N_{dmoPTA} atoms. The Cu1-O1 bond length (Cu1-O$_{DMF}$: 2.001 Å) is in concordance with those found in the literature for Cu-O$_{DMF}$ complexes (Cu-O$_{DMF}$: 1.988(10) Å) [46]. There are only few examples of DMF-Cu (II) complexes containing a DMF solvate [47], but to the best of our knowledge none of them containing two similar complexes differing only in the coordination of the DMF molecule.

Some interesting structural features of **3·3$_{DMF}$** include bond angles similar to those observed for tetranuclear Ru_2-Cu_2 complex [{RuCp

$(PPh_3)_2$-μ-dmoPTA-1κ*P*:2κ^2-*N,N*′-CuCl}$_2$-μ-Cl-μ-OCH_3]$(CF_3SO_3)_2$·(-$CH_3OH)_4$ in which the metals display also a trigonal-bypiramidal geometry [51]. The bond angle of the axial N1-Cu1-O1 is 174.07°, the average for equatorial bonds is 119,7(5,8)° (N2-Cu1-Cl3 = 121.60(2)°; N2-Cu1-Cl4 = 113.85(2)°; Cl3-Cu1-Cl4 = 123.58(14)°), being 93.1 (4.4)° (N1-Cu1-N2 = 88.68(3)°; N1-Cu1-Cl3 = 95.17(2)°; N1-Cu1-Cl4 = 95.61(2)°) the average axial-equatorial angles. The different coordination geometries of the Cu in both complexes lead to significant differences not only in the bond angles but also in the bond lengths between the metal and the ligands. The average of Cu1—Cl bond lengths in **3** (2.236(21) Å) is significant shorter than in **3$_{DMF}$** (2.337(14) Å), tendency that is also observed for the Cu1-N_{dmoPTA} bond distances (**3**: 2.009 Å; **3$_{DMF}$**: 2.070 Å).

Complex **4** crystallized in the space group $P2_1/c$, displaying a structure similar to complex **3** but with a Pd instead of a Cu. In complex **4**, the Ru moiety, exhibits a distorted pseudo-octahedral coordination sphere around the Ru atom, comprising an η^6-coordinated *p*-cymene, two chlorides and one dmoPTA ligand coordinated through the phosphorus atom. Additionally, the dmoPTA ligand coordinates a palladium atom via the CH_3N_{dmoPTA} atoms, resulting in a distorted but nearly ideal square-planar geometry around Pd, with average bond angles of 90.0 (±4.3)°. The bond angles and length are in agreement with those observed for the analogue Ru—Pd complex [RuCp$(PPh_3)_2$-μ-dmoPTA-1κ*P*:2κ^2-*N,N*′-$PdCl_2$](CF_3SO_3) in which the palladium centre also adopts a square-planar geometry [48]. The coordination of a {MCl_2} moiety in **3**·**3$_{DMF}$** and **4** through the N_{CH3} atoms leads to a better alignment between the methyl groups (C6-N1-N2-C7 dihedral angle: 0.35/1.92 (**3**/**3$_{DMF}$**), 1.79° (**4**)) with respect to complex **2** (6.68°). Also, the bigger Pd metal centre leads to some distortion of the dmoPTA ligand, thus a longer N1-N2 distance is observed for complex **4** with respect to **3**·**3$_{DMF}$** (mean **3**·**3$_{DMF}$**: 2.879(15) Å, **4**: 2.946 Å).

Finally, distances among molecules are longer than the half of the sum of their Van der Waals radii, both in complexes **2, 3**·**3$_{DMF}$** and **4**, indicating that there are not significant interactions among them.

3.3. *Stability studies of complexes **1**, **3** and **4** in solution*

Evaluation of the cytotoxic activity of the complexes in the cellular culture medium requires their dissolution. Tumor cell culture medium is mainly constituted by water, but when the complex is not soluble enough, it is previously dissolved in DMSO. It is important to determine if these complexes are the real active antiproliferative species in solution, so the study of the stability was performed at room temperature and 37 °C and monitored by $^{31}P\{^1H\}$ NMR. Complex **1** is soluble in water by quick decomposition while is more stable in DMSO. The complexes **3** and **4** are enough soluble in water and DMSO to study the stability of their dissolutions in both solvents.

Complex **1** in water at room temperature transformed into new species within just 5 min. A deeper study of the evolution of complex **1** was carried out but at 37 °C (**Fig. S21**), which is the physiological temperature. After dissolution, three species were observed at $\delta^{31}P$ = −10.21 ppm (71 %), −9.08 ppm (19 %), and that corresponding to **1** at $\delta^{31}P$ = −15.12 ppm (10 %) that disappeared after 30 min, remaining only the two other signals in a proportion of 25 % and 75 % up to 12 h. The most intense signal at $\delta^{31}P$ = −10.21 ppm is due to the complex [$RuCl_2$(η^6-*p*-cym)(HdmoPTA-κ*P*)]$^+$ that is obtained from **1** by elimination of the methylene group between the CH_3N atoms of the dmPTA ligand by reaction with water, which leads to the formation of the ligand dmoPTA and formaldehyde (Scheme 2) [17]. The presence of formaldehyde in the reaction was confirmed by a singlet at 4.75 ppm in the ^1H NMR of the reaction corresponding to its hydrated form ($CH_2(OH)_2$). It is important to point out that the signal at $\delta^{31}P$ = −9.08 ppm (25 %) disappeared when four equivalents of NaCl were introduced in the dissolution, supporting that this signal is due to mono-aquo complex [RuCl(η^6-*p*-cym)(OH_2)(HdmoPTA-κ*P*)]$^{2+}$. This equilibrium between the complex and water molecules was also observed for mono and *heterobimetallic* RAPTA complexes in water [16,17]. In DMSO at room temperature, a similar behaviour can be observed but over longer periods of time (**Fig. S22**). After 30 min, it is possible to observe the signal corresponding to the complex [$RuCl_2$(η^6-*p*-cym)(HdmoPTA-κ*P*)]$^+$ at −8.97 ppm (7 %), which increased to reach 40 % after 72 h. Unlike what was observed in water, there is no sign of the presence of the mono-aquo complex.

Complex **3** is soluble in water ($S_{25°C,H2O}$ = 9.5 mg/cm^3) and DMSO ($S_{25°C,DMSO}$ = 49.5 mg/cm^3). The dissolution of this complex in water leads to the almost immediate releasing of $CuCl_2$ and the complex [$RuCl_2$(η^6-*p*-cym)(HdmoPTA-κ*P*)]$^+$, which remained stable in D_2O at room temperature and 37 °C and after 24 h, as only one singlet at $\delta^{31}P$ = −10.23 ppm (**Fig. S23, S24**) ascribable to this complex was observed. This complex is not active against the cells studied as it was shown in a precedent paper [17], and therefore this is the reason for the lack of antiproliferative activity of **3**. In DMSO the complex **3** is also quite stable as the $^{31}P\{^1H\}$ NMR in this solvent after 12 h at room temperature displays a main peak at −9.09 ppm (97 %) and another in quite minor proportion at −20.2 ppm (3 %) (**Fig. S25**), while at 37 °C the same pattern of signals is observed when the dissolution is just prepared, but the signal at $\delta^{31}P$ = −20.2 ppm increased up to 12 % after 24 h (**Fig. S26**).

Complex **4** is well soluble in DMSO ($S_{25°C,DMSO}$ = 40.5 mg/cm^3) but also enough soluble in water ($S_{25°C,H2O}$ = 7.8 mg/cm^3) to study its dissolutions by NMR. The $^{31}P\{^1H\}$ NMR spectra in water at both room temperature and 37 °C show two peaks with similar intensity at −10.11 ppm and − 10.9 ppm (**Fig. S27, S28**). To determine if this particular pattern was produced by the formation exchange of the Ru—Cl atom by a water molecule to give rise to a Ru-OH_2 complex, four equivalents of NaCl were introduced into the dissolution of **4** in water. The $^{31}P\{^1H\}$ NMR spectra of the resulting solutions displayed only a singlet at −10.11 ppm, which supports that the observed signal at −10.9 ppm observed in the dissolution of **4** in water, is probably due to the complex [RuCl(η^6-*p*-cym)(OH_2)-μ-(dmoPTA-1κ*P*:2κ^2*N,N*′-$PdCl_2$]. The signals and their proportion remain unvaried after 12 h, both at room temperature and 37 °C. The $^{31}P\{^1H\}$ NMR spectra of **4** in DMSO displays a singlet at −10.44 ppm that remains unchanged after 12 h at room temperature (**Fig. S29**), while at 37 °C minor signals at −9.06 ppm (7 %), −7.63 ppm (3 %) and 8.05 ppm (3 %) were observed after 24 h (**Fig. S30**).

The dissolutions of **1**, **3** and **4**, proceeding from the stability tests,

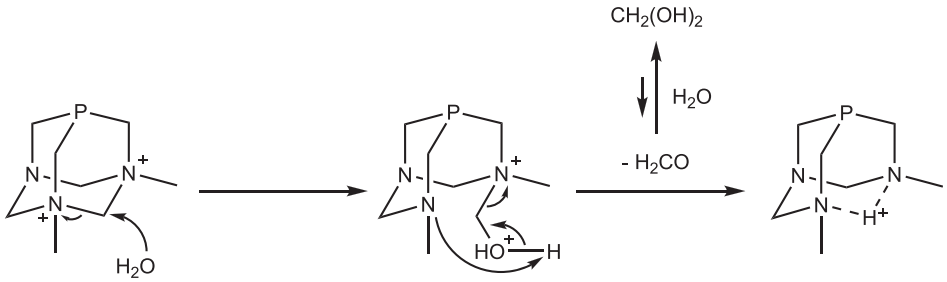

Scheme 2. Elimination of the CH_2 group between CH_3N_{dmoPTA} atoms by reaction with water, giving rise to the ligand HdmoPTA and formaldehyde.

were also evaluated by ESI-MS (**Fig. S31-S46**). The analysis of the results shows that in these dissolutions; the main component is the complex [$RuCl_2(\eta^6$-*p*-cym)(dmoPTA-κ*P*)], but other species, such as adducts in various aquation states of this complex, were also observed (*assignment in SI*). Also, it is important to point out that minoritarian species ascribable to bimetallic systems Ru—Cu and Ru—Pd were observed in the dissolutions of **3** and **4**, respectively (*assignment in SI*).

3.4. Studies of antiproliferative activity

Complexes were evaluated against the human colon adenocarcinoma cell line Caco-2/TC7 using the MTT assay [41,45]. The assessment time was 72 h. This cell type is advantageous for studying anticancer effects in cells (5 days post-seeding) and observing cells that naturally and uniformly differentiate into enterocytes [52,53]. The resulting differentiated state, which is obtained 15 days post-seeding, forms a distinctive brush border on the apical surface along with tight junctions. As a monolayer, these cells closely resemble the absorptive cells of the small intestine in morphology, enabling evaluation of the complexes' cytotoxicity and selectivity in normal epithelial-like cells [54]. Cancer and normal cells were treated with increasing concentrations of the metallic derivatives (0–20 μM). Fig. 2 shows that complexes **1**, **3**, **4** and RAPTA-C neither affect the viability of normal cells nor exhibit antiproliferative activity against cancer cells. These results are apparently contradictory with our previous conclusions in which the *heterobimetallic* complexes [$RuCl_2(\eta^6$-*p*-cym)-μ-dmoPTA-1κ*P*:2κ^2*N,N*′-MCl_2] (M = Zn, Co, Ni) [17] were found to be significantly more active that starting ruthenium complexes [$RuCl_2(\eta^6$-*p*-cym)(HdmoPTA-κ*P*)](CF_3SO_3) and **2**, and RAPTA-C against the same cell line. Excellent antiproliferative activity found for the parent complex [{$RuCp(PPh_3)_2$-μ-dmoPTA-1κ*P*:2κ^2-*N,N*′-$CuCl$}$_2$-μ-Cl-μ-OCH_3](CF_3SO_3)$_2$·(CH_3OH)$_4$ [51], in which also a Ru atom is linked by the dmoPTA to a {$CuCl_2$} moiety, showed a very high antiproliferative activity (e.g. $IC_{50} = 20 \pm 7.8$ nM against T-47D breast cells). These findings suggested that the combination of the Ru complex moiety containing *p*-cymene and dmoPTA with Cu but also with Pd should be significantly active against cancer cells.

Nevertheless, the antiproliferative results showed that complexes **3** and **4** are not active against this cell line. These compounds are stable in water, which being the most evident property that distinguishes them from previously studied active *heterobimetallic* Ru-M complexes. Previously published results on parent complexes containing *p*-cymene and dmoPTA clearly showed that the presence of a second metal plays a crucial role in inducing significant antiproliferative activity, being better than those for cisplatin and RAPTA-C. Stability experiments revealed that these bimetallic complexes are not stable enough in water and DMSO to be considered the active species interacting with the cells. In contrast, the heterometallic complexes presented in this paper are stable and do not exhibit significant antiproliferative activity against colon cancer cells. Therefore, these results suggest that the antiproliferative active species is generated by the transformation of the heterometallic complexes in cellular culture medium.

4. Conclusions

The new monometallic RAPTA-type complex [$RuCl_2(\eta^6$-*p*-cym)(dmPTA-κ*P*)](CF_3SO_3)$_2$ (**2**) and novel *heterobimetallic* complexes [$RuCl_2(\eta^6$-*p*-cym)-μ-dmoPTA-1κ*P*:2κ^2*N,N*′-M(*L*)Cl_2] (M = Cu (**3**); M = Cu, L = DMF (**3$_{DMF}$**); M = Pd (**4**)) have been synthesized and fully characterized by spectroscopic techniques. The structure of complex **2$_{Tol}$**, **3·3$_{DMF}$** and **4** have been determined by single-crystal X-ray diffraction. The crystal structure of the complex [$RuCl_2(\eta^6$-*p*-cym)(dmoPTA-κ*P*)] (**2**) confirmed that deprotonation of the HdmoPTA ligand involves a lengthening of the distance between the CH_3N_{dmoPTA} atoms, making the resulting dmoPTA ligand able to chelate metal atoms. The crystal structures of the *heterobimetallic* complexes **3·3$_{DMF}$** and **4** confirmed the ability of the {$RuCl_2(\eta^6$-*p*-cym)(dmoPTA-κ*P*)} moiety to be coordinated to a second metal through their CH_3N atoms. It is important to stress that in the crystal cell of the compound **3·3$_{DMF}$** there is two different Ru—Cu complex, with formula [$RuCl_2(\eta^6$-*p*-cym)-μ-dmoPTA-1κ*P*:2κ^2*N,N*′-$CuCl_2$](DMF) and [$RuCl_2(\eta^6$-*p*-cym)-μ-dmoPTA-κ*P*:2κ^2*N,N*′-$CuCl_2$(DMF-κ*O*)]. There are only few examples of DMF-Cu (II) complexes containing a DMF solvate, but to the best of our knowledge none of them containing two similar complexes differing only in the coordination of the DMF molecule.

Complexes **3** and **4** are sufficiently soluble and stable in water at 37 °C to allow NMR analysis. The high stability of these complexes in both water and DMSO may explain their lack of antiproliferative activity, suggesting that the active antiproliferative species are not the heterometallic complexes, but rather the products formed from their transformation in solution. These considerations encourage us to continue synthesizing new heterometallic complexes with tuned stability in aqueous solution, which could display a significant

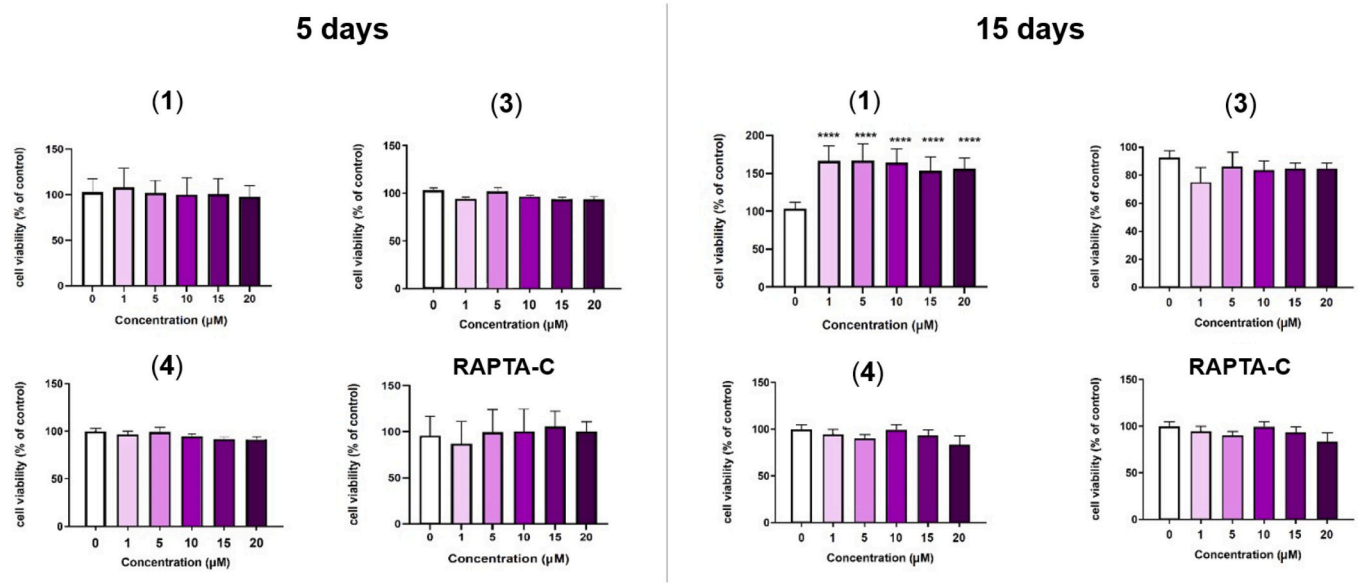

Fig. 2. Cell viability of cancer and normal Caco-2 cells (5 and 15 days after seeding, respectively) treated with complexes **1**, **3**, **4** and RAPTA-C for 72 h. All the results are expressed as mean ± SEM ($n \geq 4$ different experiments).

antiproliferative activity against colon cancer cells. The final aim being to identify the composition of the potentially active species formed in solution and to elucidate their mechanism of action.

CRediT authorship contribution statement

Nazanin Kordestani: Writing – review & editing, Investigation. **Alvaro Martinez-Aguilera:** Writing – review & editing, Investigation. **Elisa Abas:** Investigation. **Laura Grasa:** Writing – review & editing, Formal analysis. **Franco Scalambra:** Writing – review & editing, Supervision, Investigation. **Antonio Romerosa:** Writing – original draft, Supervision, Methodology, Investigation, Funding acquisition, Formal analysis.

Declaration of competing interest

The authors declare that they have no known competing financial interests or personal relationships that could have appeared to influence the work reported in this paper.

Acknowledgments

The authors thank Junta de Andalucía for funding the group PAI FQM-317 and the University of Almería for the project P_LANZ_2023/006 and P_FORT_GRUPOS_2023/94 (both projects co-funded by the European Commission FEDER program).

Appendix A. Supplementary data

Supplementary data to this article can be found online at https://doi.org/10.1016/j.ica.2025.122948.

Data availability

The data that support the findings of this study are available in the supporting information of this article.

SI Nasi-Alvaro-3.9 (Original data) (riUAL)

References

[1] B.S. Murray, P.J. Dyson, Recent progress in the development of organometallics for the treatment of cancer, Curr. Opin. Chem. Biol. 56 (2020) 28–34, https://doi.org/10.1016/j.cbpa.2019.11.001.

[2] M.R. Gonchar, E.M. Matnurov, T.A. Burdina, O. Zava, T. Ridel, E.R. Milaeva, P. J. Dyson, A.A. Nazarov, Ruthenium (II)–arene and triruthenium-carbonyl cluster complexes with new water-soluble phopsphites based on glucose: synthesis, characterization and antiproliferative activity, J. Organomet. Chem. 919 (2020) 121312, https://doi.org/10.1016/j.jorganchem.2020.121312.

[3] F. Scalambra, P. Lorenzo-Luis, I. de los Rios, A. Romerosa, New achievements on C-C bond formation in water catalyzed by metal complexes, Coord. Chem. Rev. 443 (2021) 213997, https://doi.org/10.1016/j.ccr.2021.213997.

[4] P. Servin, R. Laurent, M. Tristany, A. Romerosa, M. Peruzzini, F. Garcia-Maroto, J.-P. Majoral, A.-M. Caminade, Dual properties of water-soluble Ru-PTA complexes of dendrimers: catalysis and interaction with DNA, Inorg. Chim. Acta 470 (2018) 106–112, https://doi.org/10.1016/j.ica.2017.04.044.

[5] A.K. Singh, D.S. Pandey, Q. Xu, P. Braunstein, Recent advances in supramolecular and biological aspects of arene ruthenium (II) complexes, Coord. Chem. Rev. 270 (2014) 31–56, https://doi.org/10.1016/j.ccr.2013.09.009.

[6] B.S. Murray, M.V. Babak, C.G. Hartinger, P.J. Dyson, The development of RAPTA compounds for the treatment of tumors, Coord. Chem. Rev. 306 (2016) 86–114, https://doi.org/10.1016/j.ccr.2015.06.014.

[7] S. Swaminathan, J. Haribabu, N. Balakrishnan, P. Vasanthakumar, R. Karvembu, Piano stool Ru (II)-arene complexes having three monodentate legs: a comprehensive review on their development as anticancer therapeutics over the past decade, Coord. Chem. Rev. 459 (2022) 214403, https://doi.org/10.1016/j.ccr.2021.214403.

[8] D.J. Daigle, A.B. Pepperman, S.L. Vail, Synthesis of a Monophosphorus Analog of hexamethylenetetramine, J. Heterocyclic Chem. 11 (1974) 407–408, https://doi.org/10.1002/jhet.5570110326.

[9] J. Bravo, S. Bolaño, L. Gonsalvi, M. Peruzzini, Coordination chemistry of 1,3,5-triaza-7-phosphaadamantane (PTA) and derivatives. Part II. The quest for tailored ligands, complexes and related applications, Coord. Chem. Rev. 254 (5–6) (2010) 555–607, https://doi.org/10.1016/j.ccr.2009.08.006.

[10] C. Lidrissi, A. Romerosa, M. Saoud, M. Serrano-Ruiz, L. Gonsalvi, M. Peruzzini, Stable, water-soluble Pta-based Ru–ag organometallic polymers, Angew. Chem. Int. Ed. 44 (17) (2005) 2568–2572, https://doi.org/10.1002/anie.200462790.

[11] F. Scalambra, B. Sierra-Martin, M. Serrano-Ruiz, A. Fernandez-Barbero, A. Romerosa, First exfoliated Ru–Ru–au organometallic polymer with layered structure, Chem. Commun. 56 (66) (2020) 9441–9444, https://doi.org/10.1039/D0CC04325G.

[12] A. Mena-Cruz, P. Lorenzo-Luis, A. Romerosa, M. Saoud, M. Serrano-Ruiz, Synthesis of the Water Soluble Ligands dmPTA and dmoPTA and the Complex [RuClCp(HdmoPTA)(PPh$_3$)](OSO$_2$CF$_3$) (dmPTA = N,N'-Dimethyl-1,3,5-triaza-7-phosphaadamantane, dmoPTA = 3,7-Dimethyl-1,3,7-triaza-5-phosphabicyclo [3.3.1] nonane, HdmoPTA = 3,7-H-3,7-Dimethyl-1, 3, 7-triaza-5-phosphabicyclo [3.3.1] nonane), Inorg. Chem. 46 (15) (2007) 6120–6128, https://doi.org/10.1021/ic070168m.

[13] Z. Mendoza, P. Lorenzo-Luis, M. Serrano-Ruiz, E. Martín-Batista, J.M. Padrón, F. Scalambra, A. Romerosa, Synthesis and antiproliferative activity of [RuCp(PPh$_3$)$_2$ (HdmoPTA)](OSO$_2$CF$_3$)$_2$ (HdmoPTA = 3,7-H-3,7-dimethyl-1,3,7-triaza-5-phosphabicyclo [3.3.1] nonane), Inorg. Chem. 55 (16) (2016) 7820–7822, https://doi.org/10.1021/acs.inorgchem.6b01207.

[14] Z. Mendoza, P. Lorenzo-Luis, F. Scalambra, J.M. Padrón, A. Romerosa, One step up in antiproliferative activity: the Ru-Zn complex [RuCp(PPh$_3$)$_2$-μ-dmoPTA-1κP:2κ^{2}N, N'-ZnCl$_2$](CF$_3$SO$_3$), Eur. J. Inorg. Chem. 2018 (43) (2018) 4684–4688, https://doi.org/10.1002/ejic.201800857.

[15] Z. Mendoza, P. Lorenzo-Luis, F. Scalambra, J.M. Padrón, A. Romerosa, Enhancement of the antiproliferative activity of [RuCp(PPh$_3$)$_2$(dmoPTA-1κ*P*)]+ via its coordination to one {CoCl$_2$} unit: synthesis, crystal structure and properties of [RuCp(PPh$_3$)$_2$-μ-dmoPTA-1κP: 2κ^2 N, N'-CoCl$_2$](OTF)· 0.25 H$_2$O, Dalton Trans. 46 (25) (2017) 8009–8012, https://doi.org/10.1039/C7DT01741C.

[16] G.E. Davey, Z. Adhireksan, Z. Ma, T. Riedel, D. Sharma, S. Padavattan, D. Rhodes, A. Ludwig, S. Sandin, B.S. Murray, P.J. Dyson, Nucleosome acidic patch-targeting binuclear ruthenium compounds induce aberrant chromatin condensation, Nat. Commun. 8 (1) (2017) 1–13, https://doi.org/10.1038/s41467-017-01680-4.

[17] N. Kordestani, E. Abas, L. Grasa, A. Alguacil, F. Scalambra, A. Romerosa, The significant influence of a second metal on the antiproliferative properties of the complex [Ru(η^6-C$_{10}$H$_{14}$)(Cl$_2$)(dmoPTA)], Chem. Eur. J. 28 (3) (2022) e202103048, https://doi.org/10.1002/chem.202103048.

[18] M. Serrano-Ruiz, F. Scalambra, A. Romerosa, In *Organometallic Polymers*, Advances in Organometallic Chemistry and Catalysis: The Silver/Gold Jubilee International Conference on Organometallic Chemistry Celebratory Book, Wiley Online Library, 2013, pp. 379–405, https://doi.org/10.1002/9781118742952.ch29.

[19] A.S. Abd-El-Aziz, I. Manners, Frontiers in transition metal-containing polymers, John Wiley & Sons (2007), https://doi.org/10.1002/0470086068.

[20] J.-C. Eloi, L. Chabanne, G.R. Whittell, I. Manners, Metallopolymers with emerging applications, Mater. Today 11 (4) (2008) 28–36, https://doi.org/10.1016/S1369-7021(08)70054-3.

[21] B. Sierra-Martin, M. Serrano-Ruiz, F. Scalambra, A. Fernandez-Barbero, A. Romerosa, Novel ruthenium-silver PTA-based polymers and their behavior in water, Polymers 11 (8) (2019) 1249, https://doi.org/10.3390/polym11081249.

[22] M. Serrano Ruiz, A. Romerosa, B. Sierra-Martin, A. Fernandez-Barbero, A water soluble diruthenium–gold organometallic microgel, Angew. Chem. 120 (45) (2008) 8793–8797, https://doi.org/10.1002/anie.200803232.

[23] F. Scalambra, M. Serrano-Ruiz, A. Romerosa, First water-soluble backbone Ru–Ru–Ni heterometallic organometallic polymer, Macromol. Rapid Commun. 36 (7) (2015) 689–693, https://doi.org/10.1002/marc.201400657.

[24] F. Scalambra, M. Serrano-Ruiz, D. Gudat, A. Romerosa, Amorphization of a Ru-Ru-cd-coordination polymer at low pressure, ChemistrySelect 1 (5) (2016) 901–905, https://doi.org/10.1002/slct.201600242.

[25] J. Wang, G. Ouyang, Y. Wang, X. Qiao, W.-S. Li, H. Li, 1, 3, 5-Triazine and dibenzo [b,d] thiophene sulfone based conjugated porous polymers for highly efficient photocatalytic hydrogen evolution, Chem. Commun. 56 (10) (2020) 1601–1604, https://doi.org/10.1039/C9CC08412F.

[26] A. van Niekerk, P. Chellan, S.F. Mapolie, Heterometallic multinuclear complexes as anti-Cancer agents-an overview of recent developments, Eur. J. Inorg. Chem. 2019 (30) (2019) 3432–3455, https://doi.org/10.1002/ejic.201900375.

[27] M. Abid, F. Shamsi, A. Azam, Ruthenium complexes: an emerging ground to the development of metallopharmaceuticals for cancer therapy, Mini-Rev. Med. Chem. 16 (10) (2016) 772–786, https://doi.org/10.2174/1389557515666151001142012.

[28] S.Y. Lee, C.Y. Kim, T.-G. Nam, Ruthenium complexes as anticancer agents: a brief history and perspectives, Drug Des., Dev. Ther. 14 (2020) 5375, https://doi.org/10.2147/dddt.s275007.

[29] Y.K. Yan, M. Melchart, A. Habtemariam, P.J. Sadler, Organometallic chemistry, biology and medicine: ruthenium arene anticancer complexes, Chem. Commun. 38 (2005) 4764–4776, https://doi.org/10.1039/B508531B.

[30] N. Kordestani, H.A. Rudbari, A.R. Fernandes, L.R. Raposo, P.V. Baptista, D. Ferreira, G. Bruno, G. Bella, R. Scopelliti, J.D. Braun, Antiproliferative activities of diimine-based mixed ligand copper (II) complexes, ACS Comb. Sci. 22 (2) (2020) 89–99, https://doi.org/10.1021/acscombsci.9b00202.

[31] N. Kordestani, H.A. Rudbari, A.R. Fernandes, L.R. Raposo, A. Luz, P.V. Baptista, G. Bruno, R. Scopelliti, Z. Fateminia, N. Micale, Copper (ii) complexes with tridentate halogen-substituted Schiff base ligands: synthesis, crystal structures and investigating the effect of halogenation, leaving groups and ligand flexibility on antiproliferative activities, Dalton Trans. 50 (11) (2021) 3990–4007, https://doi.org/10.1039/D0DT03962D.

[32] S. Zhang, C. Tu, X. Wang, Z. Yang, J. Zhang, L. Lin, J. Ding, Z. Guo, Novel cytotoxic copper (ii) complexes of 8-aminoquinoline derivatives: crystal structure and different reactivity towards glutathione, Eur. J. Inorg. Chem. 2004 (20) (2004) 4028–4035, https://doi.org/10.1002/ejic.200400357.
[33] A.I. Matesanz, E. Jimenez-Faraco, M.C. Ruiz, L.M. Balsa, C. Navarro-Ranninger, I. E. León, A.G. Quiroga, Mononuclear pd (ii) and Pt (ii) complexes with an α-N-heterocyclic thiosemicarbazone: cytotoxicity, solution behaviour and interaction versus proven models from biological media, Inorg. Chem. Front. 5 (1) (2018) 73–83, https://doi.org/10.1039/C7QI00446J.
[34] M.D. Coskun, F. Ari, A.Y. Oral, M. Sarimahmut, H.M. Kutlu, V.T. Yilmaz, E. Ulukaya, Promising anti-growth effects of palladium (II) saccharinate complex of terpyridine by inducing apoptosis on transformed fibroblasts in vitro, Bioorg. Med. Chem. 21 (15) (2013) 4698–4705, https://doi.org/10.1016/j.bmc.2013.05.023.
[35] N. Kordestani, H.A. Rudbari, I. Correia, A. Valente, L. Côrte-Real, M.K. Islam, N. Micale, J.D. Braun, D.E. Herbert, N. Tumanov, Heteroleptic enantiopure pd (ii)-complexes derived from halogen-substituted Schiff bases and 2-picolylamine: synthesis, experimental and computational characterization and investigation of the influence of chirality and halogen atoms on the anticancer activity, New J. Chem. 45 (20) (2021) 9163–9180, https://doi.org/10.1039/D1NJ01491A.
[36] H.A. Rudbari, N. Kordestani, J.V. Cuevas-Vicario, M. Zhou, T. Efferth, I. Correia, T. Schirmeister, F. Barthels, M. Enamullah, A.R. Fernandes, Investigation of the influence of chirality and halogen atoms on the anticancer activity of enantiopure palladium (II) complexes derived from chiral amino-alcohol Schiff bases and 2-picolylamine, New J. Chem. 46 (14) (2022) 6470–6483, https://doi.org/10.1039/D2NJ00321J.
[37] M. Bennett, T.N. Huang, T. Matheson, A. Smith, S. Ittel, W. Nickerson, (η^6-hexamethylbenzene)ruthenium complexes, Inorg. Synth. 21 (1982) 74–78, https://doi.org/10.1002/9780470132524.ch16.
[38] G.M. Sheldrick, SHELXT - integrated space-group and crystal-structure determination, Acta Crystallogr. 71 (2015) 3–8, https://doi.org/10.1107/S2053273314026370.
[39] G.M. Sheldrick, Crystal structure refinement with SHELXL. *Acta Cryst., sect. C*, Struct. Chem. 71 (2015) 3–8, https://doi.org/10.1107/S2053229614024218.
[40] O.V. Dolomanov, L.J. Bourhis, R.J. Gildea, J.A. Howard, H. Puschmann, OLEX2: a complete structure solution, refinement and analysis program, J. Appl. Crystallogr. 42 (2009) 339–341, https://doi.org/10.1107/S0021889808042726.
[41] J. Mesonero, L. Mahraoui, M. Matosin, A. Rodolosse, M. Rousset, E. Brot-Laroche, Expression of the hexose transporters GLUTI-GLUT5 and SGLTI in clones of Caco-2 cells, Biochem. Soc. Trans. 22 (1994) 681–684, https://doi.org/10.1042/bst0220681.
[42] F. Zucco, A.F. Batto, G. Bises, J. Chambaz, A. Chiusolo, R. Consalvo, H. Cross, G. Dal Negro, I. de Angelis, G. Fabre, F. Guillou, S. Hoffman, L. Laplanche, E. Morel, M. Pincon-Raymond, P. Prieto, L. Turco, G. Ranaldi, M. Rousset, Y. Sambuy, M.L. Scarino, F. Torreilles, A. Stammati, An inter-laboratory study to evaluate the effects of medium composition on the differentiation and barrier function of Caco-2 cell lines, Altern. Lab. Anim 33 (2005) 603–618, https://doi.org/10.1177/026119290503300618.
[43] E. Abas, E. Espallargas, G. Burbello, J.E. Mesonero, A. Rodriguez-Dieguez, L. Grasa, M. Laguna, Anticancer activity of Alkynylgold(I) with $P(NMe_2)_3$ Phosphane in mouse Colon Tumors and human Colon carcinoma Caco-2 cell line, Inorg. Chem. 58 (2019) 15536–15551, https://doi.org/10.1021/acs.inorgchem.9b02528.
[44] E. Abas, R. Pena-Martinez, D. Aguirre-Ramírez, A. Rodriguez-Dieguez, M. Laguna, L. Grasa, New selective thiolate gold(i) complexes inhibit the proliferation of different human cancer cells and induce apoptosis in primary cultures of mouse colon tumors, Dalton Trans. 49 (2020) 1915–1927, https://doi.org/10.1039/C9DT04423J.
[45] T. Mosmann, Rapid colorimetric assay for cellular growth and survival: application to proliferation and cytotoxicity assays, J. Immunol. Methods 65 (1983) 55–63, https://doi.org/10.1016/0022-1759(83)90303-4.
[46] M.A. Pauly, E.M. Erwin, D.R. Powell, G.T. Rowe, L. Yang, A synthetic, spectroscopic and computational study of copper(II) complexes supported by pyridylamide ligands, Polyhedron 102 (2015) 722–734, https://doi.org/10.1016/j.poly.2015.11.015.
[47] M. Eddaoudi, J. Kim, D. Vodak, A. Sudik, J. Wachter, M. O'Keeffe, O.M. Yaghi, Geometric requirements and examples of important structures in the assembly of square building blocks, Proc. Natl. Acad. Sci. USA 99 (2002) 4900–4904, https://doi.org/10.1073/pnas.082051899.
[48] A. Alguacil, F. Scalambra, A. Romerosa, A. Bento-Oliveira, F. Marques, I. Maximiano, R. de Almeida, A.I. Tomaz, A. Valente, Evaluation of the antiproliferative properties of CpRu complexes containing N-methylated Triazaphosphaadamantane derivatives, Bioinorg. Chem. Appl. 2023 (2023) 6669394, https://doi.org/10.1155/2023/6669394.
[49] F. Scalambra, P. Lorenzo-Luis, I. de los Ríos, A. Romerosa, New findings in metal complexes with antiproliferative activity containing 1,3,5-Triaza-7-Phosphaadamantane (PTA) and derivative ligands, Eur. J. Inorg. Chem. (2019) 1529–1538, https://doi.org/10.1002/ejic.201801426, 2019.
[50] Bondi, A. van der Waals Volumes and Radii, J. Phys. Chem. 68 (1964) 441–451, https://doi.org/10.1021/j100785a001.
[51] A. Alguacil, F. Scalambra, P. Lorenzo-Luis, A. Puerta, A. González-Bakker, Z. Mendoza, J.M. Padrón, A. Romerosa, Tetranuclear Ru_2Cu_2 and Ru_2Ni_2 complexes with nanomolar anticancer activity, Dalton Trans. 52 (2023) 9541–9545, https://doi.org/10.1039/d3dt01284k.
[52] V. Meunier, M. Bourrie, Y. Berger, G. Fabre, The human intestinal epithelial cell line Caco-2; pharmacological and pharmacokinetic applications, Cell Biol. Toxicol. 11 (1995) 187–194, https://doi.org/10.1007/bf00756522.
[53] M. Rousset, The human colon carcinoma cell lines HT-29 and Caco-2: two in vitro models for the study of intestinal differentiation, Biochimie 68 (1986) 1035–1040, https://doi.org/10.1016/s0300-9084(86)80177-8.
[54] H.-P. Hauri, E.E. Sterchi, D. Bienz, J. Fransen, A. Marxer, Expression and intracellular transport of microvillus membrane hydrolases in human intestinal epithelial cells, J. Cell Biol. 101 (1985) 838–851, https://doi.org/10.1083/jcb.101.3.838.